Hindawi Publishing Corporation
Advances in Materials Science and Engineering
Volume 2012, Article ID 826873, 13 pages
doi:10.1155/2012/826873

Review Article

Nonstoichiometry in TiO_{2-y} Studied by Ion Beam Methods and Photoelectron Spectroscopy

K. Zakrzewska

Faculty of Electrical Engineering, Automatics, Computer Science and Electronics, AGH University of Science and Technology, 30 Mickiewicza Avenue, 30-059 Kraków, Poland

Correspondence should be addressed to K. Zakrzewska, zak@agh.edu.pl

Received 7 July 2011; Revised 30 August 2011; Accepted 1 September 2011

Academic Editor: Adam Georg Balogh

This paper treats a problem of nonstoichiometry in TiO_{2-y} thin films deposited by reactive sputtering at controlled sputtering rates. Ion beam techniques, Rutherford backscattering (RBS), and nuclear reaction analysis (NRA) along with X-ray photoelectron spectroscopy have been applied to determine a deviation from stoichiometry y in the bulk and at the surface of TiO_{2-y} layers. The critical review of these experimental methods is given. Defect structure responsible for the electrical resistivity of rutile TiO_2 is discussed.

1. Introduction

Titanium dioxide is considered as one of the most important materials from the point of view of both fundamental properties and applications. These applications rely on excellent chemical stability of TiO_2 in hazardous environments, hardness, high refractive index, and many other remarkable features.

Titanium dioxide TiO_2 exists in three polymorphic forms: brookite, rutile, and anatase. Anatase and brookite as metastable phases transform irreversibly into rutile over the temperature range of 973 K–1173 K [1].

Rutile is a high-temperature, stable phase, thus it is not surprising that this particular polymorphic form has been the most thoroughly investigated. The majority of crystal growth techniques yield titanium dioxide in the rutile phase. Moreover, in many devices (e.g., gas sensors) that operate at high temperatures, TiO_2 is already converted into rutile.

Recently, less common anatase has gained a considerable scientific importance thanks to a significant role it plays in photocatalytic, photovoltaic, and photoelectrochemical applications of titanium dioxide [2]. Some basic physical parameters such as the bandgap, effective mass, and mobility of charge carriers, assumed earlier to be the same as in rutile, in fact were found to differ considerably in the case of anatase.

Titanium dioxide due to its wide band gap (3.0 eV for rutile and 3.2 eV for anatase [1]) should be treated as an insulator. However, when equilibrated in an atmosphere of low oxygen activity, it becomes an oxygen-deficient semiconductor due to the electronic disorder related to nonstoichiometry [3].

Much work has been devoted to the nonstoichiometric rutile TiO_{2-y}, both in the structural aspects related to the nature of defects [4, 5] and in the subsequent physical [6, 7] and thermodynamic properties [8]. However, there is still a disagreement as to the extent of nonstoichiometry and the mechanism by which it is accommodated in rutile. It is generally believed that titania can support large deviations from stoichiometry. Earlier investigations overestimated the homogeneity range of TiO_{2-y} extending it to a value as high as $y \cong 0.1$ at 1170–1270 K [8]. Later experimental evidence [9] suggests that the homogeneity range is much narrower ($y \cong 0.008$ at 1270 K).

The structure of defects responsible for the electronic conduction in rutile and anatase TiO_2 is still a subject of discussion in spite of numerous studies devoted to this topic and the varied experimental techniques used to determine it. It is often assumed that oxygen deficiency could be accommodated by point defects: oxygen vacancies [10], titanium interstitials [11, 12], or a combination of these two defects [13]. Ionization of these defects provides electrons

necessary for the electrical conduction. Which particular defect is responsible for the electrical conductivity is largely affected by the conditions of experiment. The majority of defects switch their role when scanning over the temperature and oxygen partial pressure ranges as shown in [14].

It should be pointed out that there exists a significant controversy between two different approaches to the problem of defects in rutile. Some authors [4] claim that even for an extremely small departure from the ideal composition, nonstoichiometry is accommodated mainly by a crystallographic shear plane mechanism while the point defects model may be applied very close to the stoichiometric composition only.

Randomly distributed point defects of low density, present when the deviation from stoichiometry is small, become ordered as their concentration and interaction between them increase. In rutile (TiO_2) this ordering takes a form of planar defects, that is, crystallographic shear (CS) planes. The planar defects, when numerous enough, order to form new compounds with distinct compositions and structures known as Magnéli phases [5]. Magnéli phases constitute a homologous series with the general formula Ti_jO_{2j-1}, where j is related by $j = 1/y$ to a deviation from stoichiometry y (TiO_{2-y}).

Phase diagram of Ti–O system [1] indicates that the region of $0.1 \leq y \leq 0.25$ contains stable ordered phases Ti_jO_{2j-1} with $4 \leq j \leq 10$. For smaller departures from stoichiometry $y < 0.1$ ($10 < j < 16$) the concentration of the shear planes defects decreases and their mutual interaction becomes weaker. For a very small departure from stoichiometry, $y \cong 0.001$, corresponding to $j > 1000$, formation of isolated shear planes in equilibrium with point defects was proposed [15]. This is described as a Wadsley defect.

A detailed description of the mechanism of nucleation, growth, and aggregation of the shear planes CS is beyond the scope of this work but may be found in numerous papers devoted to this problem [4, 5, 16]. Existence of such defects in single crystals has been confirmed experimentally by STM [17] and TEM [18].

The experimental results of tracer diffusion [12], chemical diffusion [11], and thermogravimetric measurements [19] indicate titanium interstitials as the majority point defects in oxygen-deficient TiO_{2-y}. Works in favour of oxygen vacancies are also numerous. The computer simulation of the defect chemistry of rutile TiO_2 has been carried out as well [20].

This issue in the case of anatase has been only quite recently brought up [21, 22]. Na-Phattalung et al. [21] performing first-principle calculations have found that the formation energy of oxygen vacancies is higher than that of titanium interstitials. Thus, in undoped samples, titanium interstitials should be the leading donors while postgrowth formation of oxygen vacancies is also possible upon heating.

A transition from predominant oxygen vacancies to titanium interstitials in anatase has been reported by Weibel et al. [22] on the basis of the measurements of the electrical resistivity in dense anatase ceramics. This transition has been observed upon the temperature increase and/or the oxygen partial pressure decrease. Hence, it could be concluded that the formation of titanium interstitials was more favourable in anatase in comparison to rutile due to lower density of anatase than that of rutile.

Table 1: Theoretical analysis of point defects formation in TiO_{2-y}.

Majority defect	Reaction of formation	Theoretical value of m_y
Doubly ionized oxygen vacancy $V_O^{\bullet\bullet}$	$O_O^x \longleftrightarrow \frac{1}{2}O_2(g) + V_O^{\bullet\bullet} + 2e'$	6
Singly ionized oxygen vacancy $V_O^{\bullet}$	$O_O^x \longleftrightarrow \frac{1}{2}O_2(g) + V_O^{\bullet} + e'$	4
Titanium interstitial Ti_i^{4+}	$Ti_{Ti}^x + 2O_O^x \longleftrightarrow Ti_i^{4+} + 4e' + O_2(g)$	5
Titanium interstitial Ti_i^{3+}	$Ti_{Ti}^x + 2O_O^x \longleftrightarrow Ti_i^{3+} + 3e' + O_2(g)$	4

The aim of this work is to review the problem of experimental techniques best suited to the determination of deviation from stoichiometry y in TiO_{2-y} thin films. Thin films were deposited by rf and dc magnetron sputtering technique. The sputtering conditions are well defined in such a sense that the substrate temperature and sputtering rate were continuously controlled as described in detail in [23].

2. Electrical Conductivity and Point Defect Structure of TiO_{2-y}

The departure from stoichiometry y may be expressed within the ideal mass action law as a function of the oxygen partial pressure p_{O_2}:

$$y \propto {p_{O_2}}^{-1/m_y}, \tag{1}$$

where m_y yields information on the nature of the defect structure [24].

The following types of defects: doubly $V_O^{\bullet\bullet}$ and singly $V_O^{\bullet}$ ionized oxygen vacancies as well as titanium interstitials Ti_i^{3+} and Ti_i^{4+} are usually taken into account. Theoretically predicted values of m_y associated with the specific point defect are listed in Table 1. When dealing with the structure of point defects, the Kröger-Vink notation [25] is used.

The electrical conductivity of titanium dioxide is a function of the temperature, T, and oxygen partial pressure, p_{O_2}. The latter is a consequence of the relation between the departure from stoichiometry y and p_{O_2} given by (1).

The temperature dependence of the carrier concentration and conductivity for nonstoichiometric TiO_{2-y} involves the activation energy E_a of the conduction process, associated with ionization of certain neutral defects. As oxygen vacancies usually form shallow donor levels, their activation energy is much smaller than the forbidden band gap E_g and a measurable value of the electrical conductivity can be observed even at room temperature for nonstoichiometric TiO_{2-y}.

The experimental evidence shows that at high oxygen partial pressures p_{O_2}, close to 0.1 MPa and below 1200 K, TiO_2 exhibits an n-p-type transition [3, 26, 27].

In the n-type regime, the electrical conductivity σ of TiO_{2-y} is affected by the oxygen partial pressure p_{O_2}

$$\sigma \propto {p_{O_2}}^{-1/m_\sigma}. \quad (2)$$

This is due to the fact that the electron concentration n_e is a function of p_{O_2}

$${n_e} \propto {p_{O_2}}^{-1/m_n}, \quad (3)$$

which results from the relationship between n_e and the departure from stoichiometry y. When the mobility of charge carriers is independent of the oxygen partial pressure, then $m_n = m_\sigma$.

The coefficients m_y, m_n, and m_σ can be calculated from the appropriate models of point defects. Experimentally, they can be determined from the relations given by (1), (2), or (3) by measuring y, n_e, or σ, respectively, as a function of oxygen partial pressure p_{O_2}. As shown in Figure 1, the slope of $\sigma(p_{O_2})$ dependence plotted in the double logarithmic coordinate system yields the coefficient m_σ. According to the analysis presented in Table 1, it should be possible on this basis to discriminate between different types of defects and determine the majority defect mechanism.

In practice, the electrical measurements in TiO_2 over the temperature range of 1070–1370 K reveal [14] that the slope of $\log\sigma$ against $\log p_{O_2}$ is different under different regimes of oxygen activities. Therefore, the parameter m_σ associated with the majority defect, changes when p_{O_2} is varied. At low oxygen partial pressures m_σ close to 5 is obtained which can be accounted for by titanium interstitials, Ti_i^{4+}. Over the intermediate range of p_{O_2}, $m_\sigma = 6$ and doubly ionized oxygen vacancies $V_O^{\bullet\bullet}$ are postulated. Finally, at high p_{O_2} the value close to 4 is observed, corresponding to either singly ionized oxygen vacancy defect, $V_O^{\bullet}$, or interstitial titanium, Ti_i^{3+}.

In the n-p-type transition region, two competitive defect models have been proposed [26, 27]. One is related to the extrinsic disorder and assumes that the acceptor-type impurities are always present in TiO_2. The second model considers the Schottky-type defect comprising the titanium vacancy $V_{Ti}^{////}$ associated with oxygen vacancy $V_O^{\bullet\bullet}$. Both models give the same dependence of concentration of electrons (n_e) and that of holes (n_h) on p_{O_2}:

$$\begin{aligned} {n_e} &\propto {p_{O_2}}^{-1/4}, \\ {n_h} &\propto {p_{O_2}}^{1/4}. \end{aligned} \quad (4)$$

The p-type conductivity in TiO_2 is predicted to occur under very high partial pressure of oxygen. The same two models: extrinsic disorder and Schottky-type defect are discussed in this case [26]. The former assumes that the concentration of holes is much larger than that of oxygen vacancies. The latter requires the concentration of holes to be compensated by $V_{Ti}^{////}$. The results of these models are quite different. The extrinsic disorder yields the concentration of holes independent of the p_{O_2} [26]. The Schottky model gives [26]

$${n_h} \propto {p_{O_2}}^{1/5}. \quad (5)$$

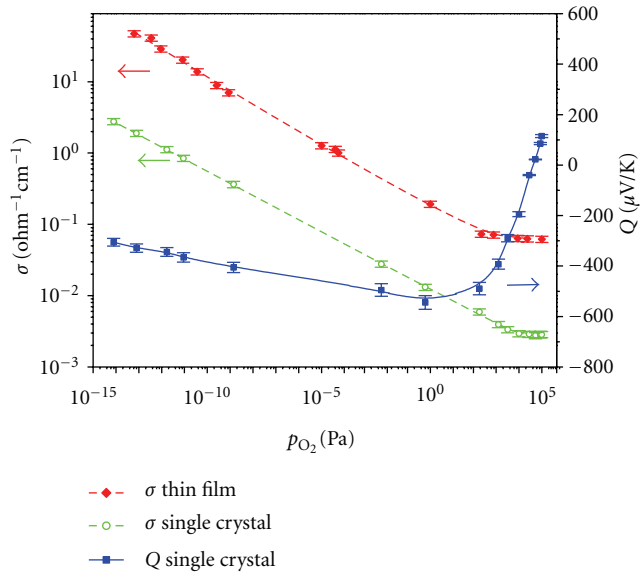

Figure 1: Electrical conductivity σ measured at 1250 K as a function of the oxygen partial pressure p_{O_2} for a thin film of TiO_{2-y}. The results of σ and Seebeck coefficient Q concern rutile single crystal.

The arguments leading to the relation described above assume a quite unrealistic situation in which only one type of defect is present. In practice, under the experimental conditions of $p_{O_2} \leq 10^5$ Pa the dependence given by (4) is observed instead.

The following comments to the analysis presented above should be taken into account.

(i) Unambiguous assignment of the majority defect on the basis of m_σ is difficult to make because frequently the same value of this parameter corresponds to more than one type of defect. This is the case for $m_\sigma = 4$ related to the singly ionized oxygen vacancy or the titanium interstitial.

(ii) Different types of majority defects predominate over different ranges of oxygen partial pressure.

(iii) One should expect the combination of point defects rather than a single defect to be present in TiO_{2-y}.

In fact, the coexistence of divalent oxygen vacancies with tri- and tetravalent titanium interstitials has been proposed [13].

3. Nonstoichiometric Thin Films of TiO_{2-y}

A variety of deposition techniques including chemical (CVD) [28–31] and physical vapour deposition (PVD) [32–34] have been reported for titanium dioxide thin films. One should mention here growth techniques successfully applied in the elaboration of TiO_2 thin films, such as sol-gel process [35], atomic layer epitaxy (ALE) [36], pulsed laser deposition [37], and filtered arc deposition (FAD) [38]. Excellent reviews, covering both the growth techniques applied to deposition of TiO_2 coatings as well as the film

morphology and optical properties, have been published [39].

Among the PVD techniques, the most important from the point of view of mass production is the sputter deposition in its multiple forms [32–34]. From all of these forms, only the reactive process, that is, the sputtering of the metallic target in oxidizing atmosphere was chosen in this work. The reason for that is the simple preparation procedure and a low cost of the target. Moreover, reactive sputtering provides thin films that are dense and uniform in thickness. It is relatively easy to control the film stoichiometry in the reactive sputtering.

The problem of nonstoichiometry is especially important in the case of thin films deposited by high-rate sputtering sources such as magnetrons. Here an uncontrollable switching between two stable modes: reactive and metallic, is likely to occur causing an abrupt change in the oxidation state of the target surface followed by modification of sputtering rate [40–43]. This affects not only a departure from stoichiometry y of TiO_{2-y} deposited thin films but the microstructure and related film properties as well.

Microstructure understood as an ensemble of physical features such as phase composition, density, porosity, roughness, and grain size is generally accepted to be the most important factor affecting the behaviour of specific devices based on thin films. This is true for gas sensors as well as for photonic and optoelectronic devices in which the electrical and optical properties of thin films are responsible for device performance. Stability of the electrical and optical responses is directly related to the microstructure changes during device operation. The control over the material microstructure is in most cases the prerequisite condition for the successful application of thin films.

3.1. Crystallographic Properties of Thin Films. It is well known that the occurrence of anatase and rutile phases in thin films depends significantly on the method and conditions of the deposition process [44–47]. There were attempts to create phase composition diagrams for thin films defining the experimental conditions under which the anatase or rutile form prevailed. The most important seem to be two such diagrams: one proposed by Pawlewicz et al. [44] and another given by Löbl et al. [47]. The work of Pawlewicz et al. [44] suggests that the phase composition is controlled by the substrate temperature and oxygen partial pressure p_{O_2}.

According to the diagram of Löbl et al. [47] (see Figure 2) modified to show the properties of the films prepared for the purposes of this work, the substrate temperature and the energy of particles impinging on the substrate, but not directly the oxygen partial pressure, are the relevant parameters that determine the film structure. The nucleation of rutile is favoured by the increasing energy transfer to the growing film and by the presence of Ti in the vapour phase.

The conclusions drawn from the above results are, however, by no means universal. As the parameters of the technological importance change from one preparation technique to another, the conditions of anatase and rutile growth should be reexamined for each particular case.

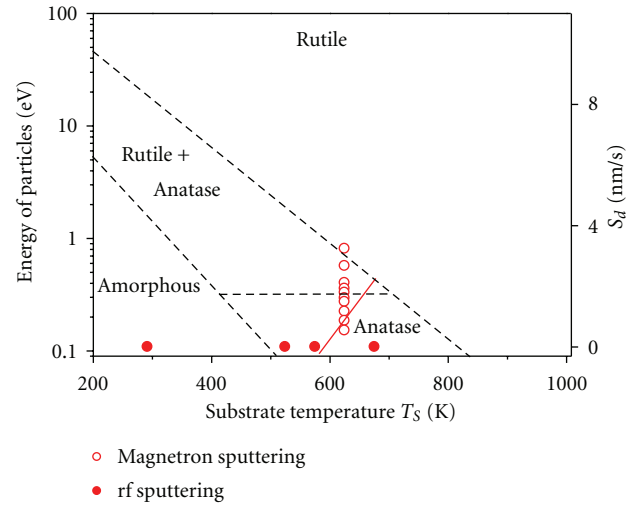

FIGURE 2: Phase composition diagram after Löbl et al. [47] modified to include the results obtained for TiO_2 thin films discussed in this work; S_d: deposition rate of thin films.

For the purposes of this work, such an analysis has been performed [23, 34, 48–51] and the results can be summarized as follows.

(i) Thin films grow as a mixture of amorphous, anatase, and rutile polymorphic forms with a varying contribution that depends on the substrate temperature and deposition rate related to oxygen partial pressure and oxidation state of the sputtered target. Low substrate temperature, low deposition rate, and oxidizing atmosphere result in anatase small crystals embedded in the amorphous background.

(ii) The contribution from the anatase TiO_2 increases with the increasing substrate temperature up to 720 K and is typical for rf sputtering at relatively low sputtering rate.

(iii) Dc magnetron sputtering at higher deposition rates yields anatase/rutile mixture. Rutile content increases with the sputtering rate under oxygen-deficient atmosphere.

3.2. Determination of the Departure from Stoichiometry y in Thin Films of TiO_{2-y}. Among many methods used to determine the chemical composition of a thin film, only some of them are sensitive enough to small negative or positive deviation from ideal stoichiometric composition (y in the formula TiO_{2-y}). These methods of microanalysis comprise Rutherford backscattering (RBS), analysis by nuclear reactions (NRA), and X-ray photoelectron spectroscopy (XPS). Traditionally employed methods of chemical analysis of elements such as electron microprobe (EMP) or energy-dispersive spectroscopy (EDS) have been used in this work but with a moderate success as they are not particularly destined for determination of oxygen nonstoichiometry.

Both RBS and NRA use the same experimental configuration that consists of an analyzed sample placed in

a monoenergetic beam of protons, deuterons, or helium ions, typically $^4He^{++}$ [52–57]. Particles coming from the bombarded sample as a result of the interaction of the beam and the elements in the sample are detected and analyzed. In the case of RBS, it is the energy of the backscattered particles that dissipated their incident energy by elastic (Rutherford) collisions, while for NRA, the energy of the reaction products is analyzed. XPS is a method that makes use of the X-ray radiation to excite electrons from the core levels of atoms [58]. Kinetic energy of the photoelectrons measured directly in XPS is related to their binding energy in atoms, which in turn is sensitive to the atom environment. The chemical shift in the binding energy forms a basis for the identification of elements and their oxidation states in the specific chemical compounds.

RBS and NRA measurements were carried out at a beam line of the 2 MeV Van de Graaff accelerator being at the disposition of GIP (Groupe de Physique des Solides) at Ecole Normale Supérieure, in collaboration with LOS (Laboratoire d'Optique des Solides) Université P. et M. Curie, Paris 6, France, described in detail in [54]. The energy of particles was measured with a silicon surface-barrier detector and the signals were analyzed with a multichannel analyzer. Complementary RBS measurements were performed at California Institute of Technology CalTech, USA. In this work, the RBS experiments were done mostly with alpha particles $^4He^{++}$ of the incident energy $E_0 = 2.012$ MeV or 1.96 MeV. The detector was placed at the scattering angle $\Theta = 165°$.

The XPS was studied at the Surface Spectroscopy Laboratory, AGH University of Science and Technology. Multitechnique setup of VSW Scientific Instruments was used.

3.2.1. RBS. Microanalysis by Rutherford backscattering (RBS) provides the ability to distinguish the atomic masses of elements and their distribution in depth as a function of the detected energy [52–56]. It is a nondestructive method, the most suitable in the case of heavy nuclei on light substrates. Typically silicon and carbon are used as substrates.

In the energy domain of the order of 2 MeV, only Coulomb interactions are responsible for the elastic scattering [52] of particles with atomic mass m at nuclei of the atomic mass M.

The energy E_1 of the ionized particle scattered at the sample surface is related to the incident energy E_0 by the laws of conservation of momentum and energy as [52, 53]

$$E_1 = K_M E_0, \tag{6}$$

with the kinematic recoil factor K_M

$$K_M = \left(\frac{m\cos\Theta + \sqrt{M^2 - m^2\sin^2\Theta}}{m + M} \right)^2. \tag{7}$$

Hence, for a given scattering geometry, the detected energy of ions scattered from the surface is a simple function of the atomic mass M of sample atom.

Equations (6) and (7) allow us to establish the position of the higher energy (leading) edge of the RBS spectrum as indicated by arrows in Figure 3. The leading edge can be further used for the identification of elements constituting the sample.

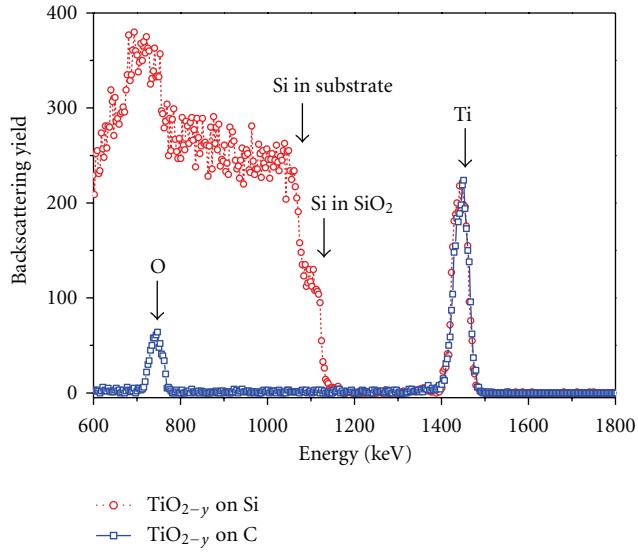

FIGURE 3: Comparison between the experimental RBS spectra of a TiO_{2-y} thin film deposited by rf sputtering on different substrates: thermally oxidized Si wafer (Si/SiO_2) and carbon foil C.

The energy difference ΔE between the position of the high and low energy edges represents the amount of energy lost by the beam on inward and outward passage through a layer. The total width ΔE of the signal is proportional to the film thickness d [52]:

$$\Delta E = [S]d, \tag{8}$$

where $[S]$ is the energy loss that depends on K_M and on the energy loss per unit path length dE/dz in a given material [52].

Equation (8) can be used to determine the thickness of layers. This is shown in Figure 3, where two experimental RBS spectra of TiO_{2-y} obtained by rf sputtering are shown. One sample was deposited on carbon foil thus enabling to observe clearly O peak (the atomic mass of carbon is smaller than that of oxygen). Simultaneously, the TiO_{2-y} thin film was deposited onto Si wafer thermally oxidized to form a thin layer of SiO_2. Thickness of this layer of about 160 nm was calculated from the width of the step shown on the Si edge in the RBS spectrum. The error in the evaluation of the thickness is determined by the energy resolution of the detector and amounts to 10–20 nm in this case.

However, one should keep in mind that the factor $[S]$ in (8) depends on the material density ρ_{mat}. Therefore, if the layer thickness is known independently and ΔE is derived from the RBS spectrum, then $[S]$ can be used to calculate the energy loss per unit length dE/dz from

$$[S]_{\text{Ti}}^{\text{TiO}_2} = K_{\text{Ti}} \left.\frac{dE}{dz}\right|_{\text{in}}^{\text{TiO}_2} + \frac{1}{|\cos\Theta|} \left.\frac{dE}{dz}\right|_{\text{out}}^{\text{TiO}_2}. \tag{9}$$

Table 2: Summary of the microanalysis of TiO_{2-y} by RBS and NRA; S_d: deposition rate, d: film thickness, N_O: surface number of oxygen atoms, N_{Ti}: surface number of titanium atoms, ρ_{mat}: film density; calculated density of anatase $\rho_A = 3.864\,g/cm^3$ and calculated density of rutile $\rho_R = 4.250\,g/cm^3$ according to [1].

Sample/substrate	Deposition method	Time (sec)	S_d (nm/s)	d (nm)	$N_O \times 10^{17}$ (at/cm^2) from NRA	$N_O \times 10^{17}$ (at/cm^2) from RBS	$N_{Ti} \times 10^{17}$ (at/cm^2) from RBS	ρ_{mat} (g/cm^3) from RBS
Na1/C	dc magnetron sputtering	41	1.43	58–60	3.25	3.03	1.58	3.17–3.39
Na2/C	dc magnetron sputtering	48	1.17	54–58	3.36	3.20	1.52	3.67–3.94
Na3/C	dc magnetron sputtering	57	0.98	52–58	3.41	3.09–3.22	1.43	3.67–4.09
Na4/C	dc magnetron sputtering	72	0.76	54–56	3.16	2.79	1.40	3.22–3.33
Na5/C	dc magnetron sputtering	95	0.54	50–52	2.53	2.69–2.74	1.31	3.15–3.27
Na6/C	dc magnetron sputtering	143	0.23	32–34	2.45	2.48	1.16	3.35–4.60
M50/C	rf sputtering	2750	0.02	50–60	3.54	2.93	1.57	3.27–3.92
M50/Si/ SiO_2	rf sputtering	2750	0.02	50–60	7.95	—	1.6	3.27–3.92
WO_1/Si	rf sputtering	15000	0.02	300	17	—	9.13	3.7

The energy loss factor $[S]_{Ti}^{TiO_2}$ of TiO_2 for scattering from Ti is composed of two terms: $K_{Ti}(dE/dz)|_{in}^{TiO_2}$ that represents the energy loss of particles on their inward path and $(1/|\cos\Theta|)(dE/dz)|_{out}^{TiO_2}$ that corresponds to the outgoing factor.

The energy loss dE/dz is, in turn, related to the number of atoms n_{Ti} in the cubic centimetre and through it to the material density ρ_{mat}. This relation is expressed by the stopping cross-section ε_{stop} defined as

$$\varepsilon_{stop} = \frac{1}{n_{Ti}}\frac{dE}{dz} = \frac{M}{N_A}\frac{1}{\rho_{mat}}\frac{dE}{dz}, \tag{10}$$

where n_{Ti} is the number of target atoms per unit volume, M is their atomic mass, and N_A is the Avogadro number.

The stopping cross section described by (10) expresses the energy loss based on the number of atoms per square centimetre.

The values of ε_{stop} are tabulated for all elements [53, 59, 60] while for compounds such as TiO_2 the stopping cross section ε_{TiO_2} is given as a sum of the elemental contributions:

$$\varepsilon_{TiO_2} = \varepsilon_{Ti} + 2\varepsilon_O. \tag{11}$$

Density ρ_{mat} can be found from (10) when the energy loss dE/dz is known from (9) and the stopping cross section is calculated from (11). This procedure has been adopted for determination of the density of the deposited thin films of TiO_{2-y} as there is no reason to assume the density equal to that of the bulk rutile or anatase. The film thickness can be taken from the profilometry and ellipsometry. The error in thickness determination is the major source of the inaccuracy of the estimated values of the density.

The results of the analysis are given in Table 2. The lowest values of ρ_{mat} correspond to the density of the amorphous TiO_2 [38], slightly higher ρ_{mat} is obtained for the mixture of anatase and rutile. The samples, the results of which are presented in Table 2, do not contain a single phase of the most elevated density (rutile).

The quantitative RBS microanalysis yields the number of atoms X per square centimetre of the target, N_X, either from the height or from the area of the corresponding peak [52]. The area A_X under the peak is proportional to the total number of atoms N_X per unit area and to the differential scattering cross section $d\sigma/d\Omega$. The absolute value of N_X requires a careful calibration, and therefore the procedure adopted in this work is based on the following formula:

$$N_X = N_{ref}\frac{A_X}{A_{ref}}\frac{(d\sigma/d\Omega)_{ref}q_{ref}}{(d\sigma/d\Omega)_X q_X}, \tag{12}$$

where the subscripts ref denote a reference sample (Bi implanted into Si) of the known concentration N_{ref}. The integrated charge q of the incident beam is usually the same for the reference sample and the studied material, $q_{ref} = q_X$. This procedure entails a systematic error in the calculated atomic concentrations of the order of 5%.

The RBS technique was applied to determine the following:

(i) surface number of titanium atoms in at/cm^2 (N_{Ti}),

(ii) surface number of oxygen atoms in at/cm^2 (N_O),

(iii) the atomic ratio O/Ti related to the departure from stoichiometry y,

(iv) film density (ρ_{mat}),

for a series of TiO_{2-y} deposited by plasma emission controlled dc-pulsed reactive magnetron sputtering and by rf reactive sputtering at different growth rates S_d (see Table 2). Oxygen can be best analyzed by RBS when the samples are deposited on C foil.

The obtained RBS spectra (e.g., in Figure 3) indicate that the samples are homogeneous and are not contaminated by foreign species. The amount of build-in argon is negligible.

3.2.2. NRA. Two basic advantages of nuclear reactions with respect to the RBS are that they provide background-free detection of light elements on heavier substrates and that they allow a perfect discrimination between two isotopes of the same element [54, 57]. Nuclear reaction analysis (NRA) is a complementary technique used for elements with low atomic number Z, like oxygen ($Z = 8$), where RBS loses sensitivity due to the Z^2 dependence of the cross section. Nuclear reactions are induced by charged particles such as protons and deuterons. The observed reaction products could be the charged particles that are detected and analyzed with the same apparatus as for RBS. Detailed information on this technique may be found in reviews [54, 57].

In this work, NRA was applied to determine oxygen concentration in thin films of TiO_{2-y}. The $^{16}O(d,p)^{17}O^*$ reaction produced by a deuteron beam with the incident energy of 850 keV was analyzed at an angle of 150°.

Typical NRA spectra of thin oxide films are shown in Figure 4. Apart from the basic reaction $^{16}O(d,p)^{17}O^*$ used for oxygen determination, two other nuclear reactions, $^{16}O(d,p)^{17}O$ and $^{12}C(d,p)^{13}C$, take place. The large peak in Figure 4(c) is related to the $^{12}C(d,p)^{13}C$ reaction in the carbon substrate.

In order to perform the quantitative analysis, only the area of the peak of $^{16}O(d,p)^{17}O^*$ is taken into account. It is then compared to the corresponding peak area of a reference sample (Ta_2O_5 thin film) of the known oxygen content.

Table 2 lists the results of the RBS and NRA analysis. Figure 5 gives the atomic ratio O/Ti for a series of TiO_{2-y} obtained by reactive sputtering as a function of the sputtering rate S_d. There is a fairly good agreement between the surface number of oxygen atoms N_O determined from NRA and RBS (Table 2). However, one should keep in mind that NRA is much more sensitive to oxygen than RBS. Systematic dependence between the sputtering rate S_d and the surface number of titanium atoms N_{Ti} is observed for a given set of samples (Na) deposited by dc magnetron sputtering (Table 2). For the purpose of keeping the same thickness for a whole set of samples, the time of deposition was adjusted accordingly. Metallic mode of deposition results in higher S_d and yields in a consequence larger content of Ti in the film. It is interesting to note that neither N_O (Table 2) nor O/Ti (Figure 5) follow the systematic dependence on S_d. For the intermediate S_d one observes a maximum in O/Ti that corresponds to the maximum in the film density derived from the RBS measurements (Table 2). The general feeling is that there is a strong correlation between the oxygen content N_O and the film density ρ_{mat}. This may be due to the amorphous nature of very thin films of TiO_2. Changes in the film density in thicker samples are due to the systematic variation in anatase/rutile ratio as a function of the sputtering rate.

3.2.3. XPS. X-ray photoelectron spectra (XPS) were recorded using a VSW Scientific Instruments electron spectrometer

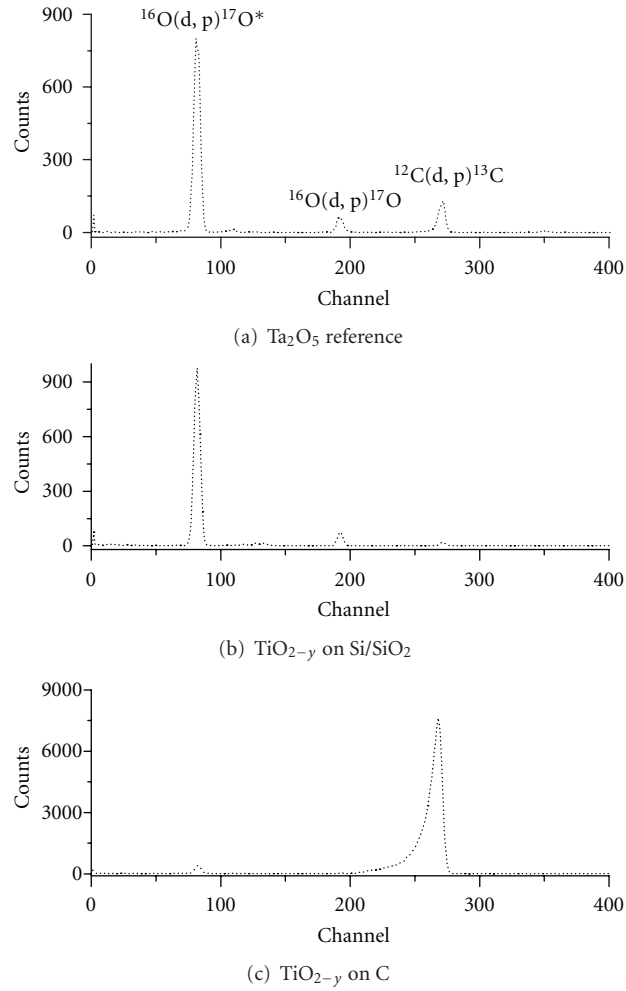

FIGURE 4: The NRA spectra of (a) Ta_2O_5 reference sample; (b) TiO_{2-y} thin film deposited on thermally oxidized Si wafer (Si/SiO_2) and (c) TiO_{2-y} on carbon foil C. The nuclear reactions corresponding to three peaks in the spectra are indicated.

fitted with a dual anode MgK_α (1253.6 eV) and AlK_α (1486.6 eV) as a source of X-ray radiation. The anode was operated at 200 W (10 kV, 20 mA). The XPS/AES chamber was equipped with a hemispherical analyzer HA150 (diameter 150 cm) at a constant pass energy of 22 eV and a multichannel detector (18 channels, 1.8 kV operating voltage). The photoelectrons were collected at a constant take-off angle. The binding energy shifts due to the surface charging were corrected assuming the C 1s XPS peak at 285.0 eV [61–63]. The position of C 1s line served as an internal standard for calibration of the binding energy scale.

The depth of XPS analysis is limited by the length of the escape path of the photoelectrons, which in turn amounts to about 2 nm for Ti $2p_{3/2}$ [64]. Taking into account a monolayer thickness of TiO_2 to be 0.22 nm it was estimated that only 10% of the total emission resulted from the surface atoms [65]. Therefore, not only the surface is probed by XPS but the subsurface layers are as well.

The objective of the XPS studies in TiO_2 is usually twofold. Primarily, it of great interest to establish the

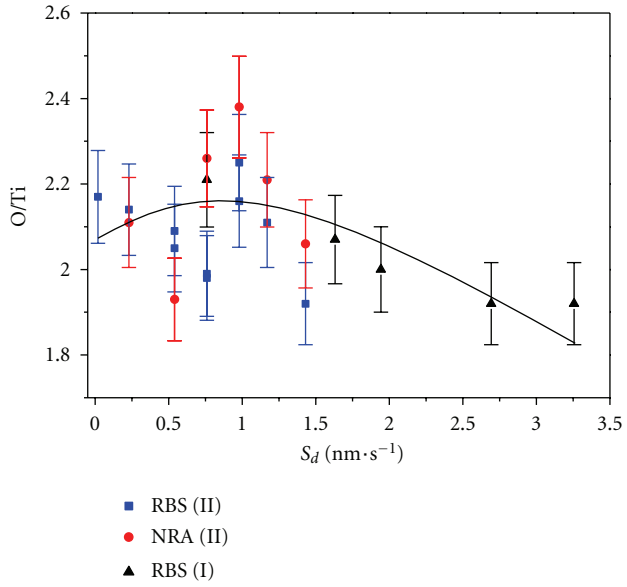

Figure 5: Atomic ratio of O/Ti, as determined by RBS and NRA, for two sets (I, II) of TiO_{2-y} thin films deposited by sputtering at different growth rates S_d . Sets I and II have different film thickness, I: 100–130 nm, II: 30–60 nm. The solid line is a guide to the eye.

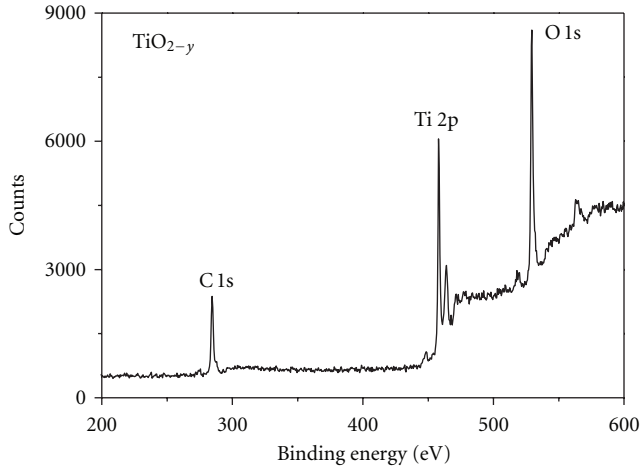

Figure 6: Typical overall XPS spectrum for a TiO_{2-y} thin film deposited by reactive sputtering onto Si wafer.

oxidation state of Ti ions. Not only Ti^{4+} related to TiO_2 but also lower oxidation states due to the presence of titanium suboxides have been reported in the literature [63, 65–72]. The first detailed study by Carley et al. [68] devoted to the step-by step oxidation of Ti metal provided evidence for intermediate oxidation states Ti^{2+} and Ti^{3+}. As to the second objective of the XPS investigations, it is of equal importance to establish the relative surface composition of elements C_X as well as to monitor the evolution of the O/Ti atomic surface ratio with deposition parameters. This requires the quantitative analysis of XPS spectra preceded by smoothing, deconvolution, and fitting of the relevant peaks. The corresponding peak area A_X is then divided by the respective relative sensitivity factors S_X [73, 74] according to the formula:

$$C_X = 100\frac{A_X/S_X}{\sum_i A_i/S_i}, \tag{13}$$

where the summation is extended over all elements in the sample.

In this work the sensitivity factors S_X were assumed to be equal to the corresponding normalized photoelectric cross-sections $S_{C\,1s} = 1$, $S_{O\,1s} = 2.93$, and $S_{Ti\,2p} = 7.91$ [75].

Figure 6 shows a survey spectrum of a TiO_{2-y} thin film deposited by sputtering. The spectrum contains the most prominent $2p_{3/2}$ and $2p_{1/2}$ lines of Ti, O 1s and C 1s at standard positions. The carbon contamination is almost impossible to avoid [73, 76]. Fortunately, it is usually limited to the film-air interface.

The binding energies of Ti $2p_{3/2}$ and O 1s core levels are listed in Table 3. The detailed analysis of the oxygen and titanium XPS peaks is presented in Figures 7 and 8.

Figure 7 shows Ti 2p doublet measured in thin films deposited under oxidizing conditions controlled by sputtering rate S_d. Two limiting cases are shown: $S_d = 1.82$ nm/s that yields substoichiometric oxides and $S_d = 0.23$ nm/s that corresponds to overoxidized conditions. The measured Ti 2p doublet is shifted by approximately 5 eV towards higher binding energy as compared with the metal. The binding energy shift of this value indicates that both films contain titanium at the highest oxidation state Ti^{4+} [68]. Almost symmetrical shape of Ti 2p peak is observed in the case of samples obtained at $S_d < 1.5$ nm/s. Formally, however, apart from Ti^{4+} related to TiO_2, one can expect at least Ti^{3+} and Ti^{2+} oxidation states as a result of the deviation from stoichiometry already discussed in this work. The substantial contributions from lower oxidation states (Ti^{3+} or Ti^{2+} and Ti^0) are seen for the samples obtained at $S_d = 1.82$ nm/s which indicates the largest oxygen deficiency. Therefore, the experimental spectra have been refined assuming a three-component structure with each component assigned to a different oxidation state, as shown in Figure 7. The relative contributions to the Ti $2p_{3/2}$ photoelectron peak have been calculated, and the results of the quantitative analysis are listed in Table 4.

The assignment of each of the three components forming Ti 2p XPS peak is difficult to make, especially because in the literature there is a large scatter of binding energies of Ti^{3+} and Ti^{2+} (see Table 3). The charging effects in thin insulating films complicate the problem.

In this work, the relative shifts of each of the fitted components have been compared to those observed in the literature (Table 3). The highest and the lowest energy components have been assigned to Ti^{4+} and Ti^0, respectively, while the intermediate component has the energy shift relative to TiO_2 that falls in between that of Ti^{3+} and Ti^{2+}. Therefore, Ti^{3+} and Ti^{2+} cannot be resolved without ambiguity.

In conclusion, the contributions from the lower oxidation states of Ti can be neglected in samples obtained with the sufficient amount oxygen in the sputtering process (at $S_d < 1.5$ nm/s). The presence of small amounts of Ti^{3+} or Ti^{2+}

Table 3: Binding energies of Ti $2p_{3/2}$ and O 1s states for TiO_{2-y} thin films deposited by reactive sputtering as compared to the literature data.

Binding energy (eV)						Reference
O_{II}	O_I	Ti^{4+}	Ti^{3+}	Ti^{2+}	Ti^0	
531.9	529.7	458.5	455.8		453.5	Reactive sputtering $S_d = 0.23$ nm/s
531.9	530.0	458.6	456.3		453.9	Reactive sputtering $S_d = 1.82$ nm/s
—	—	459.0	457.5	455.3	453.9	[68]
532.0	530.3	459.4	457.9	455.4	454.2	[63]
532.4	530.1	458.5	456.7	455.9	—	[62]
—	—	458.5	456.3	—	453.8	[70]
—	—	458.5	456.8	455.0	—	[71]
—	529.5	457.9	456.6	—	—	[67]
Binding energy shifts (eV) relative to Ti^{4+}						
		0.0	−2.7		−5.0	Reactive sputtering $S_d = 0.23$ nm/s
		0.0	−2.3		−4.7	Reactive sputtering $S_d = 1.82$ nm/s
		0.0	−1.9	−3.5	−5.3	[66]
		0.0	−1.5	−3.8	−4.7	[65]
		0.0	−1.5	−3.5	−5.1	[68]

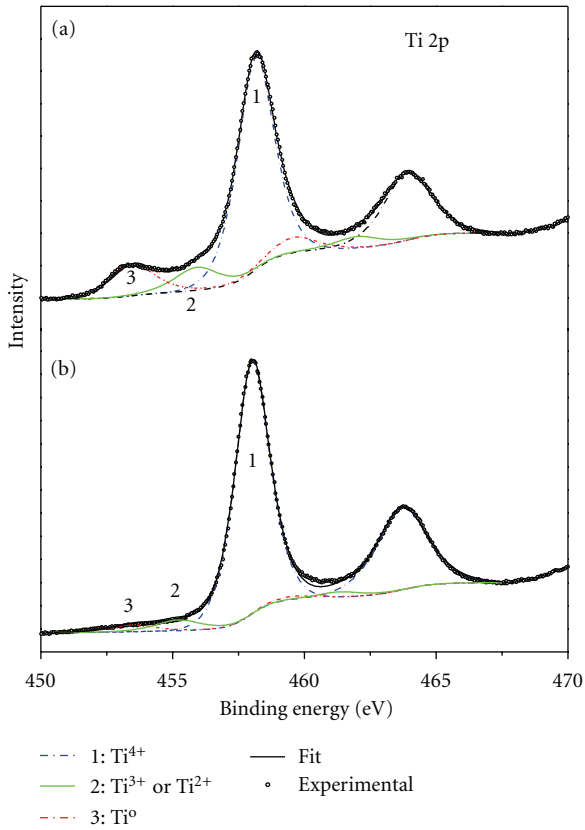

Figure 7: Fit of Ti 2p XPS spectrum for thin films of TiO_{2-y} obtained at (a) $S_d = 1.82$ nm/s and (b) $S_d = 0.23$ nm/s. Three components of each fit 1, 2, 3 correspond to different oxidation states of titanium.

Table 4: Relative contributions (%) to the Ti $2p_{3/2}$ and O 1s XPS lines from the different oxidation states for TiO_{2-y} thin films deposited by the reactive sputtering.

S_d (nm/s)	O_{II}	O_I	$O_{II}/(O_I + O_{II})$	Ti^{4+}	Ti^{3+}/Ti^{2+}	Ti^0
1.82	19	81	0.19	75.4	10.5	14.1
0.88	15	85	0.15	91.5	5.1	3.4
0.23	13	87	0.13	91.9	4.7	3.4

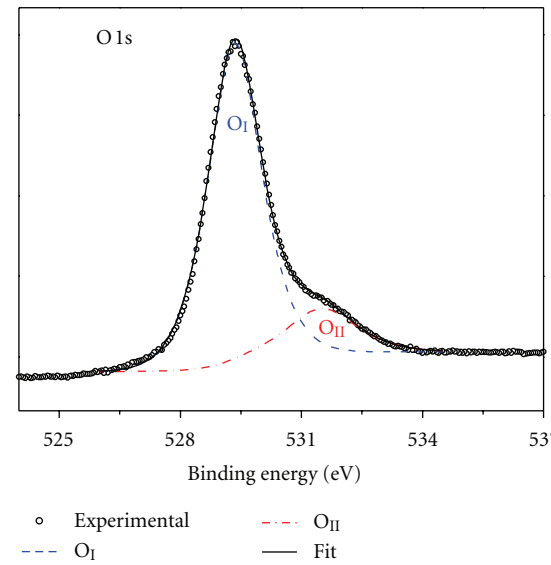

Figure 8: Fit of O 1s XPS peak for a TiO_{2-y} thin film deposited by reactive sputtering onto Si wafer at $S_d = 0.23$ nm/s.

in the films that are not completely oxidized ($S_d = 1.82$ nm/s) cannot be excluded.

Oxygen O 1s lines are asymmetrical in all studied samples which suggest that oxygen occurs in two different chemical states at least. The O 1s line could be resolved into two contributions: O_I and O_{II} (see Figure 8 and Table 4).

The binding energy of O_I state matches the literature value [63, 74] and corresponds to oxygen that occupies the normal lattice sites in the TiO_2 structure. Thus, the O_I

state represents bulk oxygen. The O_{II} state of higher binding energy could not be classified unambiguously. It is often assumed that oxygen in the surface state is responsible for the high-energy component of the asymmetrical O 1s line [69]. High-energy component has been assigned to oxygen bonded to Ti^{+3} ($O–Ti^{3+}$) [62]. However, the most probable is the argument involving the presence of hydroxyl species (OH) that are easily formed at the surface of oxide films [62, 77]. It was suggested [62] that OH-group chemisorption takes place on unsaturated Ti-sites such as Ti^{3+}. This interpretation has been assumed in this work to account for the O_{II} component of XPS O 1s peak. The presence of $OH–Ti^{3+}$ species at the surface is supported by the observation that the intensity of O_{II} component increases for samples obtained at $S_d = 1.82$ nm/s (19% of the total O 1s peak area). This effect is accompanied by a significant contribution from the low-energy component to Ti 2p peak.

Meng et al. [78] have attributed the presence of O_{II} component to the porosity, on the account of the fact that it is related to the moisture that accumulates mainly in the pores or empty columns of the material. Using the ratio of $O_{II}/(O_I + O_{II})$ as a measure of the porosity it may be concluded that TiO_{2-y} thin films with the largest deviation from stoichiometry are more porous than the stoichiometric films (see Table 4).

The observed general trend in the substoichiometric films that the O 1s high-energy and Ti 2p low-energy components are formed is associated with a defect formation. The electronic charge transfer from the anion (oxygen) to the cation (titanium) increases the binding energies of oxygen, but decreases the binding energy of the titanium core electrons [65].

4. Discussion

The summary of the quantitative analysis is given in Table 5 that compares the O/Ti atomic ratio obtained from XPS with other methods. X-ray electron microprobe (EMP) underestimates the results, but it is the method that generates the largest error as far as the oxygen content is concerned. This is due to the lack of an appropriate oxygen standard for this method. On the contrary, XPS yields the highest values for O/Ti of all the methods employed in this study. The values of O/Ti from XPS, listed in Table 5, have been obtained when integrating the area of O_I component of the O 1s peak, only. The area of O_{II} component that corresponds to oxygen bound in OH^- was not taken into account. And even in this case, the resulting values of O/Ti are much higher than those expected for a perfectly stoichiometric composition. This does not remain in accordance with the literature reports that indicate the defective surface of TiO_2 [61]. The result obtained here suggests rather that the tendency to oxidation is great for the surfaces containing titanium. The exposed surface is easily oxidized. The possible systematic error in O/Ti determination from XPS could result from the relative sensitivity factors.

Ion beam techniques, RBS and NRA are better suited for determination of oxygen nonstoichiometry y in thin films of TiO_{2-y}.

Table 5: Atomic ratio O/Ti determined by four different analytical methods described in this work for TiO_{2-y} thin films obtained under controllable conditions; electron microprobe EMP was performed with X-ray microanalyzer ARL SEMQ at beam parameters: 10 kV and 0.5 μA; beam diameter on the sample 5 μm.

Analytical method	O/Ti	
	$S_d = 1.46$ nm/s	$S_d = 0.23$ nm/s
EMP	1.87	1.92
XPS	2.47	2.44
RBS	1.93	2.11
NRA	2.06	2.14

The results of all methods discussed in this review differ as they all have their specific capabilities and limitations with respect to the material system studied. For instance, nuclear reaction microanalysis (NRA) allows for a very fast determination of the absolute total amounts of light elements in thin films up to 1 μm thick [52]. On the other hand, Rutherford backscattering RBS provides information on the composition profile in depth in a nondestructive way [53]. The analysis of XPS is limited to the first (of the order of five) atomic layers close to the sample surface because of the small mean escape depth of the photoelectrons [79].

Film composition and particularly oxygen nonstoichiometry, microstructure, and surface morphology are closely related to the sputtering conditions and in a consequence affect the electrical properties.

Systematic changes in the anatase and rutile contribution in TiO_{2-y} thin films can be accounted for by the modification of the oxidation state of the sputtered Ti target and the film deposition rate. Structure dominated by anatase grains embedded in the amorphous background seems to be a result of specific growth conditions such as a low sputtering rate of the oxidized target surface. Oxygen nonstoichiometry created at high sputtering rates promotes rutile growth.

High activation energy is required for anatase-rutile formation. This transformation involves an overall contraction of the oxygen sublattice and a movement of ions so that a cooperative rearrangement of Ti^{4+} and O^{2-} occurs. Hence, it is proposed that the removal of some oxygen ions, which generates lattice vacancies, accelerates this transformation.

The electrical resistivity ρ as a function of the sputtering rate S_d is shown in Figure 9 for nonstoichiometric thin films of TiO_{2-y} obtained by reactive sputtering. It demonstrates the existing correlation between the electrical resistivity and film composition.

For fully oxidized samples, that is, at the lowest value of growth rates S_d the electrical resistance exceeds the limit of measurement. At $S_d > 1.5$ nm/s the electrical resistivity decreases to such a level that it becomes measurable even at room temperature.

As expected, with the decreasing O/Ti, that is, for increasing deviation from the oxygen stoichiometry y, TiO_{2-y} thin films become more conducting. The close relationship between ρ and y indicates that oxygen nonstoichiometry is the source of electrons in the conduction band of titanium dioxide thin films.

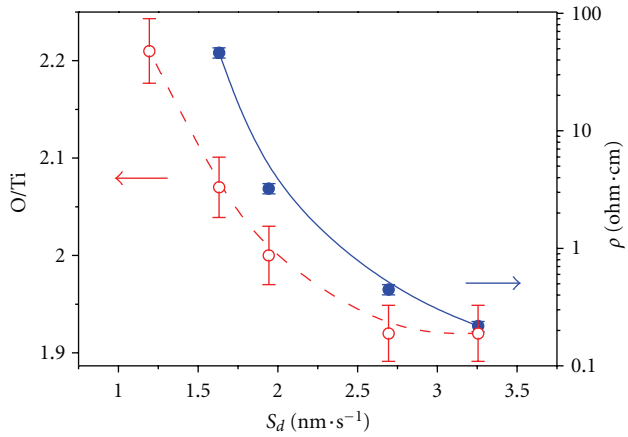

FIGURE 9: Electrical resistivity ρ at room temperature and the atomic ratio of O/Ti versus deposition rate S_d for TiO_{2-y} thin films prepared by reactive sputtering. Lines are guides to the eye.

5. Conclusions

The importance of ion beam techniques in the determination of oxygen nonstoichiometry in reactively sputtered TiO_{2-y} has been discussed in this review paper. The following detailed conclusions can be formulated:

(i) chemical composition of TiO_{2-y} thin films deposited by reactive sputtering from Ti target is close to stoichiometric but a controlled departure from stoichiometry y can be reached at a specific deposition rate;

(ii) departure from stoichiometry over the range of $-0.2 < y < 0.2$ has been found by RBS and NRA techniques while XPS, which is a typical surface analysis, yields y as high as 0.5;

(iii) film density ρ_{mat} determined from RBS measurement remains in accordance with the progressive evolution from amorphous, anatase to rutile phase and is related to the film nonstoichiometry through the surface number of oxygen atoms, N_O;

(iv) close relationship between the electrical resistivity and the deviation from stoichiometry y indicates that the oxygen deficit is a source of electrons in the conduction band.

It should be pointed out that general understanding of the problem of nonstoichiometry and its influence on the material properties is an imperative in order to make TiO_{2-y} based oxides into reliable and commercially viable electronic devices.

Acknowledgments

Special thanks are due to M. Radecka from the Department of Inorganic Chemistry, Faculty of Materials Science and Ceramics, AGH-UST for invaluable scientific contribution and fruitful discussions. The author is grateful to A. Brudnik from Department of Electronics, Faculty of Electrical Engineering, Automatics, Computer Science and Electronics, AGH-UST for preparation of dc magnetron sputtered samples; A. Brunet-Bruneau for the RBS and NRA measurements at the Laboratoire d'Optique des Solides, Universite P. et M. Curie, Paris 6, France; E. Kolawa for the RBS measurements performed at CalTech, Pasadena, USA; K. Kowalski, for XPS at the Surface Spectroscopy Laboratory, AGH-UST, Kraków, Poland. Finally, financial support from the Polish Ministry of Science and Higher Education under AGH-University of Science and Technology Grant no. 11.11.120.614 (statutory project) is acknowledged.

References

[1] L. Börnstein, "Numerical data and functional relationships in science and technology," in *Semiconductors*, O. Madelung, Ed., vol. 17, pp. 133–149, Springer, Berlin, Germany, 1983.

[2] M. A. Henderson, "A surface science perspective on TiO_2 photocatalysis," *Surface Science Reports*, vol. 66, pp. 185–298, 2011.

[3] U. Balachandran and N. G. Eror, "Electrical conductivity in non-stoichiometric titanium dioxide at elevated temperatures," *Journal of Materials Science*, vol. 23, no. 8, pp. 2676–2682, 1988.

[4] J. S. Anderson, "Shear Structures and non-stoicheiometry," in *Surface and Defect Properties of Solids*, M. W. Roberts and J. M. Thomas, Eds., p. 1, The Chemical Society, London, UK, 1972.

[5] J. S. Anderson and B. G. Hyde, "On possible role of dislocations in generating ordered and disordered shear structures," *Journal of Physics and Chemistry of Solids*, vol. 28, no. 8, pp. 1393–1396, 1967.

[6] J. F. Baumard and F. Gervais, "Plasmon and polar optical phonons in reduced rutile TiO_{2-x}," *Physical Review B*, vol. 15, no. 4, pp. 2316–2323, 1977.

[7] J. F. Baumard, D. Panis, and A. M. Anthony, "A study of TiO system between Ti_3O_5 and TiO_2 at high temperature by means of electrical resistivity," *Journal of Solid State Chemistry*, vol. 20, no. 1, pp. 43–51, 1977.

[8] R. N. Blumenthal and D. H. Whitmore, "Thermodynamic study of phase equilibria in the titanium-oxygen system within the $TiO_{1.95}$-TiO_2 region," *Journal of the Electrochemical Society*, vol. 110, pp. 92–93, 1963.

[9] J. S. Anderson and A. S. Khan, "Equilibria of intermediate oxides in the titanium-oxygen system," *Journal of the Less-Common Metals*, vol. 22, no. 2, pp. 219–223, 1970.

[10] P. Kofstad, "Thermogravimetric studies of the defect structure of rutile (TiO_2)," *Journal of Physics and Chemistry of Solids*, vol. 23, no. 11, pp. 1579–1586, 1962.

[11] N. Ait-Younes, F. Millot, and P. Gerdanian, "Isothermal transport in TiO_{2-x}. Part II. Chemical diffusion in TiO_{2-x}," *Solid State Ionics*, vol. 12, no. C, pp. 437–442, 1984.

[12] K. Hoshino, N. L. Peterson, and C. L. Wiley, "Diffusion and point defects in TiO_{2-x}," *Journal of Physics and Chemistry of Solids*, vol. 46, no. 12, pp. 1397–1411, 1985.

[13] P. Kofstad, "Note on the defect structure of rutile (TiO_2)," *Journal of the Less-Common Metals*, vol. 13, no. 6, pp. 635–638, 1967.

[14] M. Radecka and M. Rekas, "Effect of high-temperature treatment on n-p transition in titania," *Journal of the American Ceramic Society*, vol. 85, no. 2, pp. 346–354, 2002.

[15] S. Mrowec, "Extended defects in transition metals oxides," *Revue Internationale des Hautes Temperatures et des Refractaires*, vol. 14, pp. 225–242, 1977.

[16] L. A. Bursill and M. G. Blanchin, "Structure of cation interstitial defects in nonstoichiometric rutile," *Journal de Physique. Lettres*, vol. 44, no. 4, pp. L165–L170, 1983.

[17] G. S. Rohrer, V. E. Henrich, and D. A. Bonnell, "Structure of the reduced $TiO_2(110)$ surface determined by scanning tunneling microscopy," *Science*, vol. 250, no. 4985, pp. 1239–1241, 1990.

[18] M. Reece and R. Morrell, "Electron microscope study of nonstoichiometric titania," *Journal of Materials Science*, vol. 26, no. 20, pp. 5566–5574, 1991.

[19] R. T. Dirstine and C. J. Rosa, "Defect structure and related thermodynamic properties of nonstoichiometric rutile (TiO_{2-x}) and Nb_2O_5 doped rutile. II. The defect structure of TiO_2 solid solution containing 0.1–3.0 mole % Nb_2O_5 and partial molar properties for oxygen solution at 1273 K," *Zeitschrift fuer Metallkunde*, vol. 70, no. 5, pp. 322–329, 1979.

[20] C. R. A. Catlow and R. James, "Disorder in TiO_{2-x}," *Proceedings of the Royal Society of London Series A*, vol. 384, pp. 157–173, 1982.

[21] S. Na-Phattalung, M. F. Smith, K. Kim et al., "First-principles study of native defects in anatase TiO_2," *Physical Review B*, vol. 73, no. 12, Article ID 125205, pp. 1–6, 2006.

[22] A. Weibel, R. Bouchet, and P. Knauth, "Electrical properties and defect chemistry of anatase (TiO_2)," *Solid State Ionics*, vol. 177, no. 3-4, pp. 229–236, 2006.

[23] M. Radecka, K. Zakrzewska, H. Czternastek, T. Stapiński, and S. Debrus, "The influence of thermal annealing on the structural, electrical and optical properties of TiO_{2-x} thin films," *Applied Surface Science*, vol. 65-66, pp. 227–234, 1993.

[24] F. Millot, M. G. Blanchin, R. Tétot et al., "High temperature nonstoichiometric rutile TiO_{2-x}," *Progress in Solid State Chemistry*, vol. 17, no. 4, pp. 263–293, 1987.

[25] F. A. Kröger, *The Chemistry of Imperfect Crystals*, North Holland, Amsterdam, The Netherlands, 1964.

[26] J. Nowotny, M. Radecka, and M. Rekas, "Semiconducting properties of undoped TiO_2," *Journal of Physics and Chemistry of Solids*, vol. 58, no. 6, pp. 927–937, 1997.

[27] J. Nowotny, M. Radecka, M. Rekas, S. Sugihara, E. R. Vance, and W. Weppner, "Electronic and ionic conductivity of TiO_2 single crystal within the n-p transition range," *Ceramics International*, vol. 24, no. 8, pp. 571–577, 1998.

[28] S. C. Huang, T. F. Lin, S. Y. Lu, and K. S. Chou, "Morphology of and surface modification by TiO_2 deposits on a porous ceramic substrate," *Journal of Materials Science*, vol. 34, no. 17, pp. 4293–4304, 1999.

[29] K. Nishida, K. Morisawa, A. Hiraki, S. Muraishi, and T. Katoda, "In-situ monitoring of PE-CVD growth of TiO_2 films with laser Raman spectroscopy," *Applied Surface Science*, vol. 159, pp. 143–148, 2000.

[30] H. Sun, C. Wang, S. Pang et al., "Photocatalytic TiO_2 films prepared by chemical vapor deposition at atmosphere pressure," *Journal of Non-Crystalline Solids*, vol. 354, no. 12-13, pp. 1440–1443, 2008.

[31] M. L. Hitchman and F. Tian, "Studies of TiO_2 thin films prepared by chemical vapour deposition for photocatalytic and photoelectrocatalytic degradation of 4-chlorophenol," *Journal of Electroanalytical Chemistry*, vol. 538-539, pp. 165–172, 2002.

[32] S. Chaiyakun, A. Pokaipisit, P. Limsuwan, and B. Ngotawornchai, "Growth and characterization of nanostructured anatase phase TiO_2 thin films prepared by DC reactive unbalanced magnetron sputtering," *Applied Physics A*, vol. 95, no. 2, pp. 579–587, 2009.

[33] A. Brudnik, H. Czternastek, K. Zakrzewska, and M. Jachimowski, "Plasma-emission-controlled d.c. magnetron sputtering of TiO_{2-x} thin films," *Thin Solid Films*, vol. 199, no. 1, pp. 45–58, 1991.

[34] K. Zakrzewska, A. Brudnik, M. Radecka, and W. Posadowski, "Reactively sputtered TiO_{2-x} thin films with plasma-emission-controlled departure from stoichiometry," *Thin Solid Films*, vol. 343-344, no. 1-2, pp. 152–155, 1999.

[35] Z. Zainal and C. Y. Lee, "Properties and photoelectrocatalytic behaviour of sol-gel derived TiO_2 thin films," *Journal of Sol-Gel Science and Technology*, vol. 37, no. 1, pp. 19–25, 2006.

[36] A. Turković, "Grazing-incidence SAXS/WAXD on nanosized TiO_2 films obtained by ALE," *Materials Science and Engineering B*, vol. 75, no. 1, pp. 85–91, 2000.

[37] M. F. Brunella, M. V. Diamanti, M. P. Pedeferri, F. D. Fonzo, C. S. Casari, and A. L. Bassi, "Photocatalytic behavior of different titanium dioxide layers," *Thin Solid Films*, vol. 515, no. 16, pp. 6309–6313, 2007.

[38] A. Bendavid, P. J. Martin, and H. Takikawa, "Deposition and modification of titanium dioxide thin films by filtered arc deposition," *Thin Solid Films*, vol. 360, no. 1-2, pp. 241–249, 2000.

[39] P. J. Martin, "Ion-based methods for optical thin film deposition," *Journal of Materials Science*, vol. 21, no. 1, pp. 1–25, 1986.

[40] M. C. Marchi, S. A. Bilmes, C. T. M. Ribeiro, E. A. Ochoa, M. Kleinke, and F. Alvarez, "A comprehensive study of the influence of the stoichiometry on the physical properties of TiO_x films prepared by ion beam deposition," *Journal of Applied Physics*, vol. 108, no. 6, Article ID 064912, 2010.

[41] S. H. Mohamed, O. Kappertz, T. P. Leervad Pedersen, R. Drese, and M. Wuttig, "Properties of TiO_x coatings prepared by dc magnetron sputtering," *Physica Status Solidi A*, vol. 198, no. 1, pp. 224–237, 2003.

[42] A. G. Spencer and R. P. Howson, "Dynamic control of reactive magnetron sputtering: a theoretical analysis," *Thin Solid Films*, vol. 186, no. 1, pp. 129–136, 1990.

[43] E. Kinbara, E. Kusano, and S. Baba, "TiO_x film formation process by reactive sputtering," *Journal of Vacuum Science*, vol. 10, pp. 1483–1487, 1992.

[44] W. T. Pawlewicz, P. M. Martin, D. D. Hays, and I. B. Mann, "Recent development in reactively sputtered optical thin films," *Proceedings of SPIE-The International Society for Optical Engineering*, vol. 325, pp. 105–116, 1982.

[45] D. Wicaksana, A. Kobayashi, and A. Kinbara, "Process effects on structural properties of TiO_2 thin films by reactive sputtering," *Journal of Vacuum Science and Technology A*, vol. 10, pp. 1479–1482, 1992.

[46] M. H. Suhail, G. M. Rao, and S. Mohan, "Dc reactive magnetron sputtering of titanium-structural and optical characterization of TiO_2 films," *Journal of Applied Physics*, vol. 71, no. 3, pp. 1421–1427, 1992.

[47] P. Löbl, M. Huppertz, and D. Mergel, "Nucleation and growth in TiO_2 films prepared by sputtering and evaporation," *Thin Solid Films*, vol. 251, no. 1, pp. 72–79, 1994.

[48] K. Zakrzewska, A. Brudnik, E. Kusior, M. Radecka, and A. Kowal, "Microstructure of TiO_{2-x} thin films reactively sputtered by dc magnetron," in *Surface Engineering: in Materials Science I*, S. Seal, N. B. Dahotre, J. J. Moore, and B. Mishra, Eds., pp. 163–173, The Minerals, Metals & Materials Society, 2000.

[49] M. Radecka, M. Rekas, and K. Zakrzewska, "Titanium dioxide in photoelectrolysis of water," *Trends in Inorganic Chemistry, Review*, vol. 9, pp. 81–125, 2006.

[50] A. Brudnik, A. Gorzkowska-Sobaś, E. Pamuła, M. Radecka, and K. Zakrzewska, "Thin film TiO_2 photoanodes for water photolysis prepared by dc magnetron sputtering," *Journal of Power Sources*, vol. 173, no. 2, pp. 774–780, 2007.

[51] M. Radecka, M. Rekas, A. Trenczek-Zajac, and K. Zakrzewska, "Importance of the band gap energy and flat band potential for application of modified TiO_2 photoanodes in water photolysis," *Journal of Power Sources*, vol. 181, no. 1, pp. 46–55, 2008.

[52] W. K. Chu, J. W. Mayer, M.-A. Nicolet, T. M. Buck, G. Amsel, and F. Eisen, "Principles and applications of ion beam techniques for the analysis of solids and thin films," *Thin Solid Films*, vol. 17, no. 1, pp. 1–41, 1973.

[53] W. K. Chu, J. W. Mayer, and M.-A. Nicolet, *Backscattering Spectrometry*, Academic Press, London, UK, 1978.

[54] F. Abel, "Impurity analysis in solids by direct observation of nuclear reactions and elastic scattering," *Bulletin de la Societe Francaise de Mineralogie et de Cristallographie*, vol. 95, pp. 658–669, 1972.

[55] P. Mazzoldi and G. Della Mea, "The use of nuclear techniques for the analysis of thin films on glass," *Thin Solid Films*, vol. 77, no. 1–3, pp. 181–194, 1981.

[56] D. J. Oostra, "RBS and ERD analysis in materials research of thin films," *Philips Journal of Research*, vol. 47, no. 3–5, pp. 315–326, 1993.

[57] G. Amsel, J. P. Nadai, E. D'Artemare, D. David, E. Girard, and J. Moulin, "Microanalysis by the direct observation of nuclear reactions using a 2 MeV Van de Graaff," *Nuclear Instruments and Methods*, vol. 92, no. 4, pp. 481–498, 1971.

[58] D. Briggs and M. P. Seah, Eds., *Practical Surface Analysis*, vol. 1, Wiley, Chichester, UK, 2nd edition, 1990.

[59] J. F. Ziegler and W. K. Chu, "Stopping cross sections and backscattering factors for ^{4}He ions in matter," *Atomic Data and Nuclear Data Tables*, vol. 13, no. 5, pp. 463–489, 1974.

[60] http://www.srim.org/.

[61] R. Zanoni, G. Righini, A. Montenero et al., "Surface composition of alkali-doped TiO_2 films for sensors investigated by XPS," *Sensors and Actuators B*, vol. 25, no. 1–3, pp. 886–888, 1995.

[62] P. M. Kumar, S. Badrinarayanan, and M. Sastry, "Nanocrystalline TiO_2 studied by optical, FTIR and X-ray photoelectron spectroscopy: correlation to presence of surface states," *Thin Solid Films*, vol. 358, no. 1, pp. 122–130, 2000.

[63] E. McCafferty and J. P. Wightman, "An X-ray photoelectron spectroscopy sputter profile study of the native air-formed oxide film on titanium," *Applied Surface Science*, vol. 143, no. 1, pp. 92–100, 1999.

[64] M. P. Seah and W. A. Dench, "Quantitative electron spectroscopy of surfaces: a standard data base for electron inelastic mean free paths in solids," *Surface and Interface Analysis*, vol. 1, no. 1, pp. 2–11, 1979.

[65] W. Göpel, J. A. Anderson, D. Frankel et al., "Surface defects of $TiO_2(110)$: a combined XPS, XAES and ELS study," *Surface Science*, vol. 139, no. 2-3, pp. 333–346, 1984.

[66] N. R. Armstrong and R. K. Quinn, "Auger and X-ray photoelectron spectroscopic and electrochemical characterization of titanium thin film electrodes," *Surface Science*, vol. 67, no. 2, pp. 451–468, 1977.

[67] D. J. Dwyer, S. D. Cameron, and J. Gland, "Surface modification of platinum by titanium dioxide overlayers: a case of simple site blocking," *Surface Science*, vol. 159, no. 2-3, pp. 430–442, 1985.

[68] A. F. Carley, P. R. Chalker, J. C. Riviere, and M. W. Roberts, "The identification and characterisation of mixed oxidation states at oxidised titanium surfaces by analysis of X-ray photoelectron spectra," *Journal of the Chemical Society, Faraday Transactions 1*, vol. 83, no. 2, pp. 351–370, 1987.

[69] G. Rocker and W. Göpel, "Titanium overlayers on $TiO_2(110)$," *Surface Science*, vol. 181, no. 3, pp. 530–558, 1987.

[70] C. da Fonseca, S. Boudin, and M. da Cunha Belo, "Characterisation of titanium passivation films by in situ ac impedance measurements and XPS analysis," *Journal of Electroanalytical Chemistry*, vol. 379, no. 1-2, pp. 173–180, 1994.

[71] M. Sasase, K. Miyake, I. Takano, and S. Isobe, "Photocurrent performance of TiO_x films prepared by Ar+ ion beam-assisted reactive deposition method," *Thin Solid Films*, vol. 269, no. 1-2, pp. 36–40, 1995.

[72] F. Zhang, S. Jin, Y. Mao, Z. Zheng, Y. Chen, and X. Liu, "Surface characterization of titanium oxide films synthesized by ion beam enhanced deposition," *Thin Solid Films*, vol. 310, no. 1-2, pp. 29–33, 1997.

[73] J. H. Scofield, "Hartree-Slater subshell photoionization cross-sections at 1254 and 1487 eV," *Journal of Electron Spectroscopy and Related Phenomena*, vol. 8, no. 2, pp. 129–137, 1976.

[74] C. D. Wagner, W. M. Riggs, L. E. Davis, J. F. Moulder, and G. E. Mullenberg, *Handbook of X-Ray Photoelectron Spectroscopy*, Elmer Corp., Eden Prairie, MN, USA, 1979.

[75] C. D. Wagner, "Appendix 5," in *Practical Surface Analysis*, D. Briggs and M. P. Seah, Eds., vol. 1, Wiley, Chichester, UK, 2nd edition, 1990.

[76] L. J. Meng and M. P. dos Santos, "Investigations of titanium oxide films deposited by d.c. reactive magnetron sputtering in different sputtering pressures," *Thin Solid Films*, vol. 226, no. 1, pp. 22–29, 1993.

[77] K. Zakrzewska, S. Skrzypek, and J. Stoch, "Structure and composition of transparent conducting $CdIn_2O_4$ thin films," in *Proceedings of the 12th International Congress on X-ray Optics and Microanalysis, (ICXOM '89)*, S. Jasienska and L. J. Maksymowicz, Eds., vol. 2, pp. 876–879, Cracow, Poland, August, 1989.

[78] Li-Jian Meng, C. P. Moreira de Sá, and M. P. dos Santos, "Study of porosity of titanium oxide films by X-ray photoelectron spectroscopy and IR transmittance," *Thin Solid Films*, vol. 239, no. 1, pp. 117–122, 1994.

[79] C. J. Powell, "Attenuation lengths of low-energy electrons in solids," *Surface Science*, vol. 44, no. 1, pp. 29–46, 1974.